Finger Joint Characterization from X-Ray Images for Rheumatoid Arthritis Assessment

Joan M. Núñez, Débora Gil and Fernando Vilariño
Dept. of Comp. Science, Comp. Vision Center, Edifici O - UAB, 08193 Bellaterra, Spain

Keywords: Rheumatoid Arthritis, X-Ray, Hand Joint, Sclerosis, Sharp Van der Heijde.

Abstract: In this study we propose a modular system for automatic rheumatoid arthritis assessment which provides a joint space width measure. A hand joint model is proposed based on the accurate analysis of a X-ray finger joint image sample set. This model shows that the sclerosis and the lower bone are the main necessary features in order to perform a proper finger joint characterization. We propose sclerosis and lower bone detection methods as well as the experimental setup necessary for its performance assessment. Our characterization is used to propose and compute a joint space width score which is shown to be related to the different degrees of arthritis. This assertion is verified by comparing our proposed score with Sharp Van der Heijde score, confirming that the lower our score is the more advanced is the patient affection.

1 INTRODUCTION

Rheumatoid arthritis (RA) is a chronic disease that causes joint dysfunction which results, among other symptoms, in the reduction of the joint space width (JSW) and the erosion of the joint bones. Since there is not any cure for RA, the assessment of the disease becomes very important and it has led to the emergence of several semi-quantitative assessment methods. Among them, the Sharp-Van der Heijde (SvdH) score, which provides separate discrete values for JSW and bone erosion based on X-ray image examination, is the most widely used nowadays (Van der Heijde, 1999). The patient score is the sum of the scores for all the considered joints in hands and feet.

Three stages should be considered to face the automation of RA assessment: joint detection, joint characterization and joint measurements. As the main goal of this study is to propose and assess a JSW measure we will focus on the second and third stages taking hand joints as input (Figure 1). This statement leads us to a hand joint modelling to describe the necessary features to compute JSW measures. Sclerosis and lower bone appear to be the main necessary features to obtain JSW measures and the corresponding detectors are proposed.

Few previous works have faced this problem. Bielecki et al. (Bielecki et al., 2008) developed the first study that faced the challenge of a fully automatic system for RA assessment. Vera et al. (Vera, 2010) provided a method which included all the different stages of the problem improving significantly the joint detection rates. Langs et al. (Langs et al., 2009) presented a new method whose scope is also the whole RA assessment process. However, these works faced the problem as a whole stage, not modular, and did not show a clear correlation among its proposed JSW score and Svdh.

Our proposal clearly separates joint detection, joint characterization and joint measurements in three independent modules. It also provides a framework for sclerosis and lower bone detection performance assessment, and proposes a JSW score which exhibits a close relation with SvdH score. This approach allows us to confirm for the first time a relation between an automatic score and the RA disease stage. Moreover, the modular orientation of our contribution, unlike previous approaches, enables future research to specifically focus on the improvement of the different open challenges independently.

2 DATA ANALYSIS

This study is focused on the same digital database used by Vera et al. (Vera, 2010) enriched with our own manually segmented ground truth for the selected visual features necessary for JSW computation. Twenty X-ray images from different patients containing pairs of hands in posterioanterior view are avail-

Núñez J., Gil D. and Vilariño F..
Finger Joint Characterization from X-Ray Images for Rheumatoid Arthritis Assessment.
DOI: 10.5220/0004327302880292
In *Proceedings of the International Conference on Biomedical Electronics and Devices* (BIODEVICES-2013), pages 288-292
ISBN: 978-989-8565-34-1

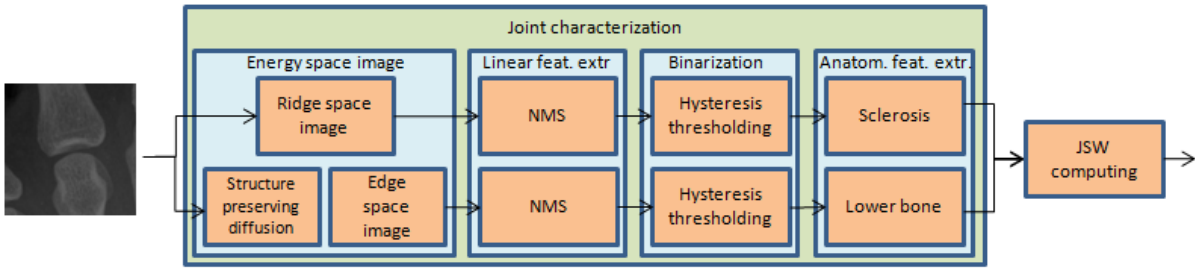

Figure 1: Rheumatoid Arthritis characterization system.

able in DICOM format, 2828x2320 resolution and intensity range from 0 to 4095. Hand joints have been marked by an expert who was asked to spot the joint middle point along the finger axis and the joint orientation. A hand joint dataset containing 560 images of joints have been created (14 joints/hand). Among these samples, a total number of 320 joints were labelled with their SvdH score for inter-phalangeal distance (discrete values from 0 to 3). These 320 samples comprised 160 metacarpo-phalangeal joints (MCP) and 160 proximal inter-phalangeal joints (PIP) -distal inter-phalangeal joints (DIP) are not considered within SvdH score-. Erosion scoring was not collected because it is out of the scope of this this study.

Our proposed hand joint model does not consider thumb joints as they represent a different problem due to its specific profile. Since images are taken with the hands in posterioanterior view -from the hand back with the palm facing down- a profile view of the thumb is taken. Consequently, a frontal projection is obtained for the rest of the fingers whereas a lateral projection is obtained for the thumbs. This reason, as well as their specific skeletal structure, causes the visual features observed in thumbs to be substantially different and justifies that they are not included in this study. As far as the other finger joints are concerned, several features are distinguished within the model: sclerosis, upper bone contour, lower bone contour and lower bone inner edges, as depicted in Figure 2 (Núñez et al., 2011). The sclerosis and the lower bone contour are the main necessary features to carry out measures on JSW. The sclerosis (feature 1 in Figure 2(b)) appears as a consequence of the upper bone shape and the way an X-ray image is created. The X-ray beam have to pass through a higher density region due to the concavity of the lower part of the upper bone of the joint (feature 2 in Figure 2(b)). As a consequence, the sclerosis appears as a prominent high intensity region. Regarding the lower bone, the visual features are also a consequence of the mentioned X-ray image acquisition mechanism and the lower bone shape (feature 3 in Figure 2(b)). That shape can vary in the different fingers or the different hand joints and the inner edges may be present or not (feature 4 in Figure 2(b)). However, the lower bone contour is defined by the outer part of the lower bone.

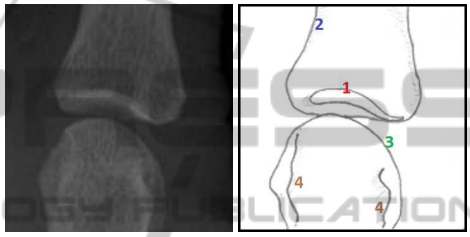

(a) (b)

Figure 2: (a) Joint example. (b) Joint model schema (1: sclerosis, 2: upper bone, 3: lower bone, 4: inner edges).

3 METHODOLOGY

Our proposed sclerosis and lower bone detectors include several stages: energy space image, linear feature extraction, binarization and anatomical feature extraction.

The first stage aims to obtain the energy space image. The intensity levels of that image describe the chances of finding a feature in every pixel. Two separate processes are achieved in order to obtain the ridge space image and the edge space image. A second derivative of anisotropic Gaussian (DoG) method is used to compute the ridge space image. This method is based on the fact that ridges can be obtained as the high values in the second derivative. We apply a bank of filters where each of them achieves a convolution with the corresponding kernel template. We design our filter templates based on second derivatives of anisotropic Gaussian kernels. Considering that an oriented Gaussian function is described by:

$$G_{(\sigma_x,\sigma_y),\theta} = \frac{1}{(2\pi)\sigma_x\sigma_y} e^{-\left(\frac{\tilde{x}^2}{2\sigma_x^2}+\frac{\tilde{y}^2}{2\sigma_y^2}\right)} \quad (1)$$

where (σ_x, σ_y) are the scales in the corresponding axis, θ is the rotation angle of the filter and $\tilde{x}$ and $\tilde{y}$

are the coordinates given by the rotation angle. Hence they are defined as:

$$\begin{aligned}\tilde{x} &= x\cos\theta + y\sin\theta \\ \tilde{y} &= x\sin\theta - y\cos\theta\end{aligned} \tag{2}$$

We use anisotropic Gaussians with $\sigma = \sigma_x = 2\sigma_y$. Therefore, the Gaussian function results in:

$$G_{\sigma,\theta} = \frac{1}{(2\pi)2\sigma^2} e^{-\left(\frac{\tilde{x}^2}{2(2\sigma)^2} + \frac{\tilde{y}^2}{2\sigma^2}\right)} \tag{3}$$

Hence the kernel will be defined as:

$$\partial^2_{\tilde{y}} G_{\sigma,\theta} = \frac{\tilde{y}^2 - 1}{\sigma^4} G_{\sigma,\theta} \tag{4}$$

We apply a normalization so that the geometry of the valleys is prioritized:

$$G^N_{\sigma,\theta} := \frac{\|\partial^2_{\tilde{y}} G_{\sigma,\theta} * I\|}{\|\partial^2_{\tilde{y}} G_{\sigma,\theta}\| \|I\|} \tag{5}$$

where $\|\cdot\|$ stands for the L^2 integral norm and $*$ denoting the convolution operator.

The kernels are applied to different scales and in different equally distributed orientations in a range centered in the joint orientation. The final outcome are 24 output images, each of them corresponding to a determined orientation and scale. Hence, the output I_{ridges} must be a combination of all of them, defined as the maximum of the outputs from each filter:

$$I_{ridges} = \max_{i,j} \left(G^N_{\sigma^i,\theta^j} \right) \tag{6}$$

On the other hand, the edge space image is obtained as the gradient of the input image after applying structure preserving diffusion (Gil et al., 2009). Diffusion filtering proved its success in improving the quality of the edge detection by smoothing the image irregularities while keeping the main image structure.

The second stage performs the feature extraction using Non-maximum Suppresion algorithm (Canny, 1986), which only keeps pixels that are local maxima along the gradient direction. Gradients are computed using the structure tensor of the space image.

In the third stage hysteresis thresholding algorithm (Canny, 1986) is used to binarize the non-maximum suppressed images while preserving feature connectivity and removing weak responses.

Finally, the two images forwarded by the third stage must go through the fourth processing step in order to provide the final sclerosis and lower bone segmentations. This stage is different for the two thresholded images:

- The final sclerosis segmentation is the ridge in the binarized image that is closer to the center of the image following the finger orientation .
- As far as lower bone is concerned, the corresponding binarized image is processed to remove the edges in the upper part and the margins. Afterwards, the endpoints in the remaining processed edges are linked. The final lower bone segmentation is obtained by computing the convex hull of the linked-edge image.

4 EXPERIMENTAL SETUP

Two subsets were created from our dataset of 320 annotated images to perform our experiments: 1) Tune Dataset, with 40 randomly selected healthy joints (20 MCP and 20 PIP); 2) Test Dataset, with the remaining 280 joints (140 MCP and 140 PIP). The Tune Dataset was used to tune the parameters of the system for sclerosis and lower bone contour segmentation, and the Test Dataset was used to compute the output of our system and compare the proposed distance measure with the SvdH score. We added 20 DIP joints from the non-annotated dataset to enrich the variability of the Tune Dataset -these joints can be safely included because, although not having a SvdH score, they fit our model-. Both sclerosis and lower bone were manually segmented by an expert using OsiriX (Rosset et al., 2004) software exclusively for the 60 images of the Tune Dataset.

Performance metrics were developed to evaluate the performance of the system, i.e. the quality of our detections, and tune the parameters. We based our metrics on the Average Surface Distance (ASD), defined as follows:

$$ASD(U,V) = \frac{1}{|S(U)|} \left(\sum_{s_U \in S(U)} d(s_U, S(V)) \right) \tag{7}$$

where, given a pixel p and a region R conformed by a set of pixels $S(R)$, $d(p,S(R))$ is defined as:

$$d(p,S(R)) = \min_{s_R \in S(R)} \|p - S_R\| \tag{8}$$

where $\|.\|$ stands for the Euclidean distance.

Thus, if A denotes our automatic segmentation and M denotes the manual delineation, we define:

$$Caught = ASD(A,M) \tag{9}$$

$$Missed = ASD(M,A) \tag{10}$$

When both Caught and Missed metrics are zero the segmentation is perfect. Caught metric value is related to the quality of the detector at detecting valid pixels (true positives) and avoiding non-desired pixels (false positives). Analogously, the lower the value of Missed, the less desired information was missed (false negatives).

Table 1: Valid sclerosis and lower bone detection rates.

	J. type	SvdH 0	SvdH 1	SvdH 2	SvdH 3	Total
Sclerosis	**MCP**	111/115 (96.5%)	10/11 (90.9%)	10/12 (83.3%)	2/2 (100.0%)	**133/140 (95.0%)**
	PIP	64/67 (95.5%)	27/35 (77.1%)	22/28 (78.5%)	5/10 (50.0%)	**118/140 (84.2%)**
	Total	**175/182 (96.1%)**	37/46 (80.4%)	32/40 (80.0%)	7/12 (58.3%)	**251/280 (89.4%)**
L. bone	**MCP**	85/115 (73.9%)	5/11 (45.4%)	8/12 (66.6%)	0/2 (0.0%)	**98/140 (70.0%)**
	PIP	42/67 (62.6%)	14/35 (40.0%)	8/28 (28.5%)	3/10 (30.0%)	**67/140 (47.8%)**
	Total	**127/182 (69.7%)**	19/46 (41.3%)	16/40 (40.0%)	3/12 (25.0%)	**165/280 (58.9%)**

Table 2: Valid sclerosis and lower bone detection rates (both in the same image).

J. type	SvdH 0	SvdH 1	SvdH 2	SvdH 3	Total
MCP	83/115 (72.1%)	5/11 (45.4%)	6/12 (50.0%)	0/2 (0.0%)	**94/140 (67.1%)**
PIP	39/67 (58.2%)	11/35 (31.4%)	6/28 (21.4%)	2/10 (20.0%)	**58/140 (41.4%)**
Total	**122/182 (67.0%)**	16/46 (34.7%)	12/40 (30.0%)	2/12 (16.6%)	**152/280 (54.2%)**

This experimental setup was used in order to train the detection systems with the Tune Dataset. The system providing the lowest values for the performance metrics was selected, giving priority to a lower Caught value so that the provided output is better although some parts may be missed. Afterwards, the selected detectors were applied to the Test Dataset. The final sclerosis and lower bone outputs were then visually tested in order to separate the wrong detections from those detections that can be useful to compute JSW scores. The final detections were accepted if they provided a good segmentation and there were not remaining spurs in the joint interspace.

Finally, the proposed JSW measurement is the minimum distance between the sclerosis and the lower bone. It is defined as:

$$d_{min} = \min_{p \in L} d(p, S) \tag{11}$$

where S and L stand for the sclerosis surface and the lower bone contour, respectively.

5 RESULTS

Table 1 shows the valid sclerosis and lower bone rates when applying our sclerosis detector to the Test Dataset. High detection rates have been obtained in the case of sclerosis detection, reaching higher rates in the case of healthy samples (SvdH 0), providing 96.1%, since they are closer to our joint model. However, these detection rates drop down to 58.3% in the case of joints in a more advanced RA stage, which makes clear the potential usefulness of the model in order to classify advanced stages of the disease. All in all, the detection rate reaches the remarkable value of 89.6% on the whole dataset. As far as MCP and PIP are concerned, the detection rates remain close

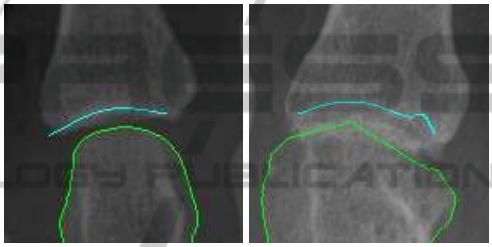

(a) (b)

Figure 3: (a) MCP valid detection. (b) MCP wrong detection.

although a light tendency is confirmed which shows that PIP joints present more detection problems.

On the other hand, lower bone detection arises as a very difficult problem. The overall detection rate drops to 58.9% although the healthy samples reach 69.7%. The lack of an stardard practice in X-ray image techniques causes an important variability in the samples which makes lower bone segmentation difficult to achieve. Figure 3 shows two detection examples of wrong and valid segmentations.

The samples where both lower bone and sclerosis segmentations were labelled as valid were considered for further analysis. Table 2 contains the corresponding results. The rates when the two segmentations are considered altogether are just slightly below the lower bone detection rates, reaching 67.0% for healthy samples and 54.2% for the whole dataset.

Afterwards, the proposed JSW measure was computed and tested in relation to SvdH score. In the case of MCP samples (Figure 4), the JSW estimation shows a light decreasing trend as the value of SvdH score increases. Nevertheless, that decreasing trend is clear in the case of PIP samples (Figure 5). It is an encouraging result taking into account that our system is only considering JSW values. Standard clinical assessment considers more information as the symme-

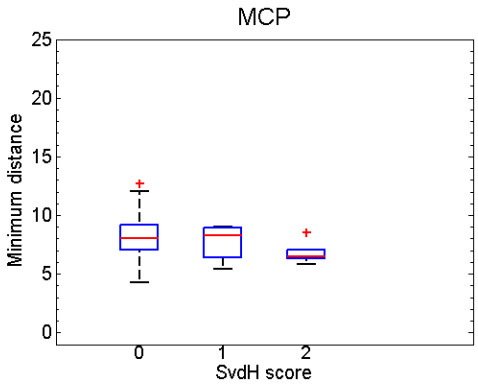

Figure 4: MCP joints, distance measure and SvdH score.

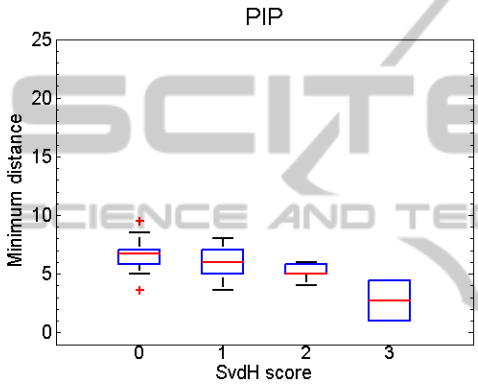

Figure 5: PIP joints, distance measure and SvdH score.

try between hand joints or erosion information.

Finally, the reliability of the proposed system to provide a proper JSW estimation independently of its relation to the RA stage was tested. The JSW measure was computed both for the manual and automatic segmentations of the Tune Dataset, providing a final error of 1 ± 0.7 pixels. This result confirms the robustness of the JSW estimation.

6 CONCLUSIONS

The proposed system sets the foundations of a modularized RA assessment system. We created a hand joint sample dataset and introduced a hand joint model based on the skeletal structure of hand bones. Our sclerosis detector achieves remarkably good results. However, lower bone segmentation appears to be a harder task when faced in a local way. The JSW measure we propose was compared with the gold standard score for RA assessment. We showed for the first time that an automatic measure for JSW can be computed so that its value has a clear relation to the SvdH manual measure assessed by clinical personnel and, therefore, to RA disease stage. Future work should involve the confirmation of this trend with a dataset which should include a larger study with samples from multiple sources. Higher SvdH score samples, particularly scarce in number should be also considered.

ACKNOWLEDGEMENTS

This work was supported in part by the Spanish Gov. grants TIN2012-33116, TIN2009-13618, MICINN TIN2009-10435 and Consolider 2010 MIPRCV (CSD2007-00018), and the UAB grant 471-01-2/2010. The second author has been supported by the Ramon y Cajal Program.

REFERENCES

Bielecki, A., Korkosz, M., and Zielinski, B. (2008). Hand radiographs preprocessing, image representation in the finger regions and joint space width measurements for image interpretation. *PRn*, 41(12):3786–3798.

Canny, J. (1986). A computational approach to edge detection. *PAMI*, (6):679–698.

Gil, D., Hernàndez-Sabaté, A., Burnat, M., Jansen, S., and Martínez-Villalta, J. (2009). Structure-preserving smoothing of biomedical images. In *Computer Analysis of Images and Patterns*, pages 427–434. Springer.

Langs, G., Peloschek, P., Bischof, H., and Kainberger, F. (2009). Automatic quantification of joint space narrowing and erosions in rheumatoid arthritis. *Medical Imaging, IEEE Transactions on*, 28(1):151–164.

Núñez, J., F., V., and D., G. (2011). Computer vision techniques for characterization of finger joints in x-ray images. Technical report, Centre de Visió per Computador.

Rosset, A., Spadola, L., and Ratib, O. (2004). Osirix: An open-source software for navigating in multidimensional dicom images. *Journal of Digital Imaging*, 17:205–216. 10.1007/s10278-004-1014-6.

Van der Heijde, D. (1999). How to read radiographs according to the sharp/van der heijde radiological assessment in rheumatoid arthritis in long term studies. *Journal of Rheumatology*, (26):743–745.

Vera, S. (2010). Finger joint modelling from hand x-ray images for assessing rheumatoid arthritis. Technical report, Centre de Visió per Computador.